Propagation of guided waves through weak penetrable scatterers

Agnès Maurel[a)]
Institut Langevin/LOA, UMR 7587, CNRS-ESPCI, 10 rue Vauquelin, 75231 Paris Cedex 05, France

Jean-François Mercier
Poems, UMR 7231, CNRS-ENSTA-INRIA, 32 bld Victor, Paris 75015, France

(Received 26 August 2011; revised 28 December 2011; accepted 5 January 2012)

The scattering of a scalar wave propagating in a waveguide containing weak penetrable scatterers is inspected in the Born approximation. The scatterers are of arbitrary shape and present a contrast both in density and in wavespeed (or bulk modulus), a situation that can be translated in the context of SH waves, water waves, or transverse electric/transverse magnetic polarized electromagnetic waves. For small size inclusions compared to the waveguide height, analytical expressions of the transmission and reflection coefficients are derived, and compared to results of direct numerical simulations. The cases of periodically and randomly distributed inclusions are considered in more detail, and compared with unbounded propagation through inclusions. Comparisons with previous results valid in the low frequency regime are proposed. © *2012 Acoustical Society of America*.
[DOI: 10.1121/1.3682037]

PACS number(s): 43.20.Fn, 43.20.Mv, 43.20.Bi [ANN] Pages: 1874–1889

I. INTRODUCTION

The interaction of guided waves with scatterers has been studied in a large variety of physical contexts. In the context of dielectric waveguides, as used in optical communication, interest lies in the understanding of the effects of impurities due to material defects and in the possibility of utilizing deliberate isolated impurities as passive optical components.[1–3] The detection and the characterization of buried defects or targets motivates research in the context of acoustic waves,[4–6] water waves,[7,8] and in the context of elastic waves.[9,10] The problem of scattering by a single scatterer centered in a waveguide is analogous to the scattering problem by a periodic array of scatterers. This latter problem has its own interest and it has been extensively studied, notably to handle for several mathematical difficulties and to develop accurate and efficient numerical methods.[11–13] Also, a recent increasing interest for these periodic structures is inspired by the success of studies of photonic crystals[14] and possible applications in other contexts of waves. The literature is vast, see Refs. 15 and 16 for recent works using a supercell approach and for a review, also see Ref. 17.

The scattering of waves by obstacles, either penetrable or not, is a complicated problem and exact analytical solutions are in general unavailable. This is why it is of common practice to employ approximation methods, for their mathematical simplicity and applicability to any shape and structure, also for the easy implementation when considering inverse problems. Among the approximate methods, the Born approximation (Debye–Ganz or Debye–Rayleigh approximation in the context of electromagnetic waves) is the most commonly used. See Refs. 18–21 regarding imaging techniques in the context of guided waves. This approximation employs the incident field as the total field in its first iteration, an approximation expected to be valid for weak scattering, namely predominant single scattering contribution [then, the $(n+1)$th iteration employs the field at the nth iteration as the total field]. Extensive literature exists on the discussion of the validity of the Born approximation. Some studies focus on theoretical aspects: Does the Born series converge and if so, how large is the error when broken off after a finite number of terms? Other studies propose a heuristic criterion for its range of validity by comparison of the approximated solution with an exact analytical result, when available, or with experiments/numerical simulations. We refer to several studies in the context of acoustic[22–25] electromagnetism[26–28] and quantum mechanics.[29,30] Because of weak scattering approximation, the range of validity concerns the low frequency regime when impenetrable inclusions are considered (sound soft/Dirichlet or sound hard/Neumann scatterers). Less attention has been paid to penetrable inclusions/scatterers, where the scattering strength results from a combination of the scatterer size and of the strength of the contrasts in density and bulk modulus for acoustic waves, ocean depth in the context of water waves, permittivity and permeability for electromagnetic waves, etc. We mention the experimental study presented in Ref. 31 on light scattering by penetrable blood cells with low contrast in the refractive index showing that the Born approximation is accurate well beyond the low frequency regime (until $kR \sim 10$–100, where k is the wavenumber and R is the blood cell size). This latter situation corresponds to weak scattering because of the weak contrast in the optical index between the cell and the surrounding aqueous medium rather than because of small scatterer size. Finally, of particular interest is Ref. 32, where an experimental method is presented to isolate in an experimental signal the contribution of single scattering from the multiple scattering contribution, offering an experimental test for the first Born approximation.

The present paper addresses the problem of acoustic i.e., scalar waves propagating in a waveguide containing a single inclusion or a set of penetrable inclusions. In the context of acoustic waves in fluid with inclusions having contrasts both

a)Author to whom correspondence should be addressed. Electronic mail: agnes.maurel@espci.fr

in density ρ and in bulk modulus B, the corresponding equation for the pressure p is

$$\nabla \cdot \left(\frac{1}{\rho(\mathbf{r})} \nabla p(\mathbf{r}) \right) + \frac{\omega^2}{B(\mathbf{r})} p(\mathbf{r}) = 0, \tag{1}$$

with continuity of p and the normal component of $\nabla p/\rho$ at the inclusion boundaries. This equation applies in other contexts of scalar waves: (i) The outplane displacement u of SH waves in solids

$$\nabla \cdot (\mu(\mathbf{r}) \nabla u(\mathbf{r})) + \rho(\mathbf{r}) \omega^2 \, u(\mathbf{r}) = 0$$

with (μ, ρ) the shear modulus and the mass density of the elastic medium, (ii) the surface elevation η for water (gravity) waves propagating in varying shallow water depth $h(\mathbf{r})$ (with g the acceleration due to gravity)

$$\nabla \cdot (h(\mathbf{r}) \nabla \eta(\mathbf{r})) + \frac{\omega^2}{g} \eta(\mathbf{r}) = 0,$$

and (iii) for the electric field E or the magnetizing field H for polarized transverse magnetic or transverse electric electromagnetic waves, with permittivity ϵ and permeability μ

$$\nabla \left(\frac{1}{\mu(\mathbf{r})} \nabla E(\mathbf{r}) \right) + \omega^2 \epsilon(\mathbf{r}) E(\mathbf{r}) = 0,$$
$$\nabla \left(\frac{1}{\epsilon(\mathbf{r})} \nabla H(\mathbf{r}) \right) + \omega^2 \mu(\mathbf{r}) H(\mathbf{r}) = 0.$$

The paper is organized as follows. In Sec. II, an integral representation for the $p_n(x)$-coefficients of the modal decomposition of the solution $p(\mathbf{r})$ is derived. The resulting Eq. (8) is the basic equation to implement numerical calculations in the successive Born approximations $p_{NBC}(x, y)$ and examples for inclusion of nontrivial shapes are given. It can be used also to derive analytical expressions of the transmission and reflection coefficients [the corresponding field is $p_B(x, y)$]. Notably, simplifications are presented when considering inclusions of any shape, but of size small compared to the waveguide height [Eq. (16), note that this assumption does not restrict the solution to the low frequency regime].

Section III presents a discussion on the validity of the predictions p_{NBC} and p_B, the reference calculations being performed using the finite element MELINA code.[33] The scattering properties are dependent on multiple parameters that are discussed. Basically, and as expected in this iterative approach, the relevant parameter to predict the accuracy of our analytical p_B and numerical p_{NBC} predictions is the amplitude of the scattered field, that results from a combination of the inclusion size and of the contrasts in wavespeed and in density. Our conclusion is that for an incident wave field of unit amplitude and denoting ϵ_s the amplitude of the scattered field p^s, our estimate p_B^s is accurate up to ϵ_s^2 for ϵ_s until values close (but smaller) than 100%. When this is the case, iterating NBC causes the solution to converge.

Finally, Sec. IV focuses on the properties of the scattering by periodic and random distributions of inclusions. In the former case, the comparison with the scattering by an unbounded infinite array of inclusions allows us to recover the usual grating law and in connection, the Wood's anomaly. Preliminary numerical experiments (much more difficult because numerical averages are needed) are presented for random distribution of inclusions. Reasonable agreement with our prediction is found. In both periodic and random configurations, comparisons with perturbative approaches in the low frequency regime are proposed.

II. INTEGRAL REPRESENTATION OF THE FIELD SCATTERED BY INCLUSIONS

In this section, we use the wave equation in an integral form together with a modal decomposition onto the transverse modes of the waveguide. Accounting for the appropriate boundary conditions at the inclusion boundaries leads to an integral representation, Eq. (8), of the modal coefficients $p_n(x)$. For weak scattering strength of the inclusions, an approximated solution is proposed using the Born approximation. This can be done numerically by iterating the successive Born solutions [Eq. (11)]. Alternatively, an analytical solution is proposed when assuming that the size of the inclusions is small compared to the height of the waveguide. Note that this latter assumption does not assume *a priori* a small inclusion size compared to the incident wavelength.

A. Description of the problem

The problem under consideration is shown in Fig. 1: An acoustic waveguide in the two-dimensional (2D) -space $\mathbf{r} = (x, y)$, with wavespeed c and mass density ρ contains inclusions that presents a contrast in density and in wavespeed with respect to the host medium $(\tilde{\rho}, \tilde{c})$. The inclusions are located within a region $0 < x < L$.

A wave is generated by a source located at $x = x_s < 0$ [encapsulated in the source term $s(\mathbf{r})$, this choice, rather than a plane wave coming from $-\infty$ will be justified later] and propagates in the waveguide. In the ω-frequency regime, the wave satisfies the wave equation

$$\nabla \cdot \left(\frac{1}{\rho(\mathbf{r})} \nabla p(\mathbf{r}) \right) + \frac{\omega^2}{B(\mathbf{r})} p(\mathbf{r}) = s(\mathbf{r}), \tag{2}$$

in the waveguide (domain Ω) where $\rho(\mathbf{r}) = \rho$ and $B(\mathbf{r}) = B \equiv \rho c^2$ and inside the inclusion (domain $\tilde{\Omega}$) where

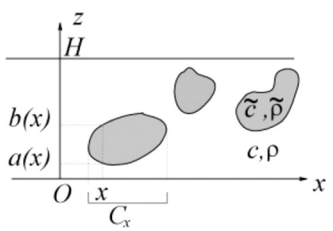

FIG. 1. Ensemble of penetrable inclusions in a waveguide and parametrization of the inclusion boundary.

$\rho(\mathbf{r}) = \tilde{\rho}$ and $B(\mathbf{r}) = \tilde{B} \equiv \tilde{\rho}\tilde{c}^2$. We also define the wavenumber $k \equiv \omega/c$. The boundary conditions on the walls of the waveguides at $y = 0, H$ are

$$\partial_y p(x,0) = \partial_y p(x,H) = 0, \tag{3}$$

and we have continuity of p and the normal component of $\nabla p/\rho$ at the boundary of the inclusion. The source term $s(x, y)$ is written as

$$s(x,y) = \frac{1}{\rho}\delta(x - x_s)\psi_N(y),$$

where $\psi_n(y)$ are the usual eigenfunctions of the waveguide

$$\begin{cases} \psi_n(y) \equiv \sqrt{2}\cos\frac{n\pi y}{H} \\ \psi_0(y) = 1, \end{cases}$$

satisfying $\partial_y\psi_n(0) = \partial_y\psi(H) = 0$ on the boundaries of the waveguide and satisfying the orthogonality relation $\int_0^H dy\ \psi_n(y)\psi_m(y) = H\delta_{nm}$. These ψ_n-functions form a basis of $H^1(0, H)$ (the function and its first derivative are square-integrable).

B. Modal decomposition and derivation of the integral representation

Before deriving the modal decomposition of the pressure, let us write problem (2) in a variational form: By multiplying Eq. (2) by a test function $q(\mathbf{r}) = Q(x)\psi_n(y)$, with $Q(x)$ compactly supported, and integrating over the whole domain of the waveguide $\Omega_t = \Omega \cup \tilde{\Omega}$, we get

$$\begin{aligned} &\int_{\Omega_t} d\mathbf{r}\left[\nabla p(\mathbf{r})\cdot\nabla q(\mathbf{r}) - k^2 p(\mathbf{r})q(\mathbf{r})\right] \\ &\quad + \int_{\tilde{\Omega}} d\mathbf{r}[(\rho/\tilde{\rho} - 1)\nabla p(\mathbf{r})\cdot\nabla q(\mathbf{r}) \\ &\quad - k^2(B/\tilde{B} - 1)p(\mathbf{r})q(\mathbf{r})] = -\rho\int_{\Omega_t} d\mathbf{r}\ s(\mathbf{r})q(\mathbf{r}). \end{aligned} \tag{4}$$

We now expand p on the ψ_n

$$p(\mathbf{r}) = \sum_m p_m(x)\psi_m(y). \tag{5}$$

The modal coefficients of ∇p are obtained accounting for the continuity of p at the boundary of the inclusion

$$\begin{cases} \int_0^H \partial_x p(x,y)\psi_m(y) = \dfrac{d}{dx}\displaystyle\int_0^H dy\ p(x,y)\psi_m(y) = Hp'_m(x) \\ \int_0^H dy\ \partial_y p(x,y)\psi'_m(y) = -\displaystyle\int_0^H dy\ p(x,y)\psi''_m(y) = \left(\frac{m\pi}{H}\right)^2 Hp_m(x), \end{cases}$$

so that ∇p can be expended on the ψ_m-functions (respectively, ψ'_m-functions)

$$\nabla p(\mathbf{r}) = \sum_m \begin{pmatrix} p'_m(x)\psi_m(y) \\ p_m(x)\psi'_m(y) \end{pmatrix}.$$

Note that we have used the fact that the $\psi'_m(y)$-functions also form a basis with $\int_0^H \psi'_m(y)\psi'_n(y) = (m\pi/H)^2\delta_{nm}$. Equation (4) becomes, using the orthogonality relations of the ψ_m and ψ'_m functions, the variational formulation

$$\begin{aligned} &\int_{-\infty}^{+\infty} dx\left[p'_n(x)Q'(x) - k_n^2 p_n(x)Q(x)\right] + \frac{1}{H}(\rho/\tilde{\rho} - 1)\sum_m \int_{-\infty}^{+\infty} dx\left[C_{nm}(x)p'_m(x)Q'(x) + D_{nm}(x)p_m(x)Q(x)\right] \\ &\quad - \frac{k^2}{H}(B/\tilde{B} - 1)\sum_m \int_{-\infty}^{+\infty} dx\ C_{nm}(x)p_m(x)Q(x) = -\int_{-\infty}^{+\infty} dx\ Q(x)\delta(x - x_s)\delta_{nN}, \end{aligned}$$

where we have defined

$$\begin{cases} k_n^2 \equiv k^2 - \left(\dfrac{n\pi}{H}\right)^2 \\ C_{nm}(x) \equiv \displaystyle\int_{a(x)}^{b(x)} dy\ \psi_m(y)\psi_n(y) = \frac{\alpha_{nm}}{2}\left[Y\ \mathrm{sinc}\frac{(n-m)\pi Y}{H} + Y\mathrm{sinc}\frac{(n-m)\pi Y}{H}\right]_{Y=a(x)}^{Y=b(x)} \\ D_{nm}(x) \equiv \displaystyle\int_{a(x)}^{b(x)} dy\ \psi'_m(y)\psi'_n(y) = nm\frac{\pi^2}{H^2}\left[Y\ \mathrm{sinc}\frac{(n-m)\pi Y}{H} + Y\mathrm{sinc}\frac{(n+m)\pi Y}{H}\right]_{Y=a(x)}^{Y=b(x)} \end{cases} \tag{6}$$

for $x \in \mathcal{C}_x$ otherwise $C_{nm}(x) = D_{nm}(x) = 0$ (for $x \notin \mathcal{C}_x$), with $\mathcal{C}_x$ the x-range containing one or more inclusions (Fig. 1). We have defined the function $\mathrm{sinc}\, x \equiv \sin x/x$, and the coefficients $\alpha_{00} = 1$, $\alpha_{n0} = \alpha_{0n} = \sqrt{2}$ for $n \neq 0$ and $\alpha_{nm} = 2$ for $m \neq 0$, $n \neq 0$. In the previous expression, $(x, a(x))$ and $(x, b(x))$ correspond to the parameterization of the interface

between one inclusion and the host medium (Fig. 1). In the case of several inclusions occupying $\tilde{\Omega} = \cup\tilde{\Omega}_i$, the result comes from linearity as a sum over all the inclusions: in Eq. (4), $\int_{\tilde{\Omega}}$ can be replaced by $\sum_i \int_{\tilde{\Omega}}$. Integrating the above-mentioned variational formulation by parts, we obtain

$$\begin{aligned} p_n''(x) + k_n^2 p_n(x) &= \frac{(\rho/\tilde{\rho} - 1)}{H} \sum_m \Big[-\big(C_{nm}(x) p_m'(x)\big)' \\ &\quad + D_{nm}(x) p_m(x) \Big] - \frac{k^2 (B/\tilde{B} - 1)}{H} \sum_m C_{nm}(x) p_m(x) \\ &\quad + \delta(x - x_s)\delta_{nN} \end{aligned} \tag{7}$$

owing to the fact that $C_{nm}(x)$ and $Q(x)$ vanish at $\pm\infty$. The one-dimensional (1D) Green's function

$$g_n(x) = \frac{e^{ik_n|x|}}{2ik_n}$$

satisfying

$$\left(\frac{\partial^2}{\partial x^2} + k_n^2\right) g_n(x - x') = \delta(x - x')$$

is used to get an integral representation of the solution $p_n(x)$ of Eq. (7)

$$\begin{aligned} p_n(x) = g_N(x - x_s)\delta_{nN} &- \frac{k^2 (B/\tilde{B} - 1)}{H} \sum_m \int_{c_x} dx' g_n(x - x') C_{nm}(x') p_m(x') \\ &+ \frac{(\rho/\tilde{\rho} - 1)}{H} \sum_m \int_{c_x} dx' \big[-g_n'(x - x') C_{nm}(x') p_m'(x') + g_n(x - x') D_{nm}(x') p_m(x') \big], \end{aligned} \tag{8}$$

where $g_n'(x - x') \equiv \partial_x g_n(x - x')$. Note that the dependence on the solution $p_n(x)$ on the shape and position of the inclusion(s) is encapsulated in the coefficients C_{nm} and D_{nm}. Incidentally, the integral representation of Eq. (7) causes a term at the boundaries $x' \to \pm\infty$ of the form $\big[\partial_{x'} g_n(x - x') p_n(x') - g_n(x - x') p_n'(x')\big]_{x' \to \pm\infty}$ to appear. Although Green's function of the 1D problem does not vanish at infinity, this term vanishes because of the form of our source term: with a source located at x_s, we have $\partial_{x'} f_n(x') = \pm i k_n f_n(x')$ for both $f_n = g_n$ or p_n when $x' \to \pm\infty$. This property causes the term at the boundaries to vanish.

In practice, we can choose the position of the source x_s outside the region containing the inclusions, say $x_s < 0$. Thus, the incident wave can be written (for $x_s < x < +\infty$)

$$p^{inc}(x, y) \equiv g_N(x - x_s)\psi_N(y) = \mathcal{A} e^{ik_N x} \psi_N(y), \tag{9}$$

which corresponds to a particular right going guided mode (mode N). In the following, without loss of generality, we choose $\mathcal{A} = 1$.

We inspect in the following section the possibility to evaluate $p_n(x)$ in the Born approximation.

C. Iterative solutions using the Born approximations

The first iteration in the Born approximation consists of identifying the total field with the incident field, leading to

$$p_n^0(x) = e^{ik_N x}\delta_{Nn}, \tag{10}$$

The expression of $p_n(x)$ in Eq. (8) can be evaluated perturbatively in the successive Born approximation, namely

$$\begin{aligned} p_n^{i+1}(x) = e^{ik_N x}\delta_{nN} &+ \frac{(\rho/\tilde{\rho} - 1)}{H} \sum_m \int_{\mathcal{C}_x} dx' \big[-g_n'(x - x') C_{nm}(x') p_m^i{}'(x') + g_n(x - x') D_{nm}(x') p_m^i(x') \big] \\ &- \frac{k^2 (B/\tilde{B} - 1)}{H} \sum_m \int_{\mathcal{C}_x} dx' \; g_n(x - x') C_{nm}(x') p_m^i(x'), \end{aligned} \tag{11}$$

where p_n^i denotes the solution in the ith-Born approximation.

Numerically, $p_n^i(x)$ can be evaluated for any inclusion shape by truncating the sums over m to some N_{mod} values (in general, at least the propagating modes are considered, the evanescent modes being relevant in the near field only), for $i = 1$ to some N_{it} order. The corresponding 2D solution $p_{NBC}(x, y)$ (NBC stands for numerical Born calculation) is

$$p_{NBC}(x, y) = \sum_{n=0}^{N_{mod}} p_n^{N_{it}}(x)\psi_n(y), \tag{12}$$

and it depends on both the number of considered modes N_{mod} and on the order of the Born approximation N_{it}. A simple implementation can be found in the Appendix.

In the following, we give typical examples of the NBC for nontrivial inclusion shapes: S_1 where the inclusion boundary (x_b, y_b) is parametrized with t using $x_b/H = 0.175 \cos t + 2.5$,

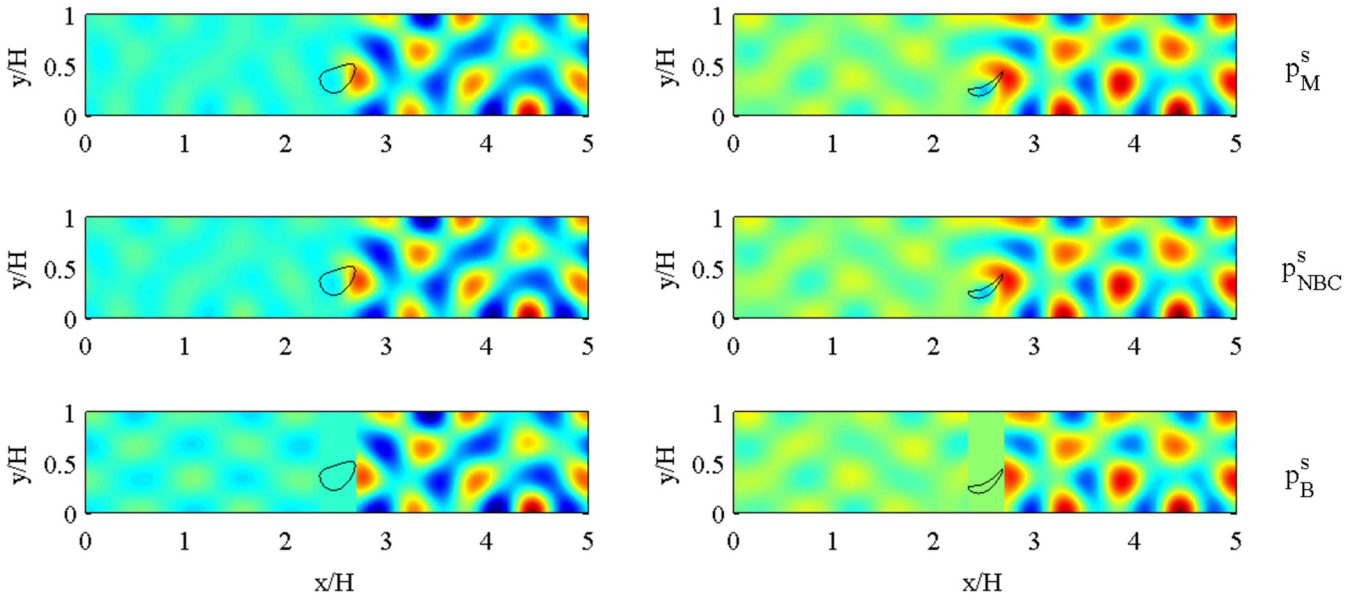

FIG. 2. (Color online) Scattered field $p^s_M(x,y)$ (top), $p^s_{NBC}(x,y)$ (middle, calculated for $N_{mod}=10$ and $N_{it}=6$) and $p^s_B(x,y)$ [bottom, calculated from Eq. (14)] for (left) the inclusion shape S_1 and (right) the inclusion shape S_2. No contrast in mass density has been considered in both cases, the contrast in wavespeed is $c/\tilde{c}=1.2$ and $kH=11.12$. The errors are, for S_1, $Er_B=9\%$, $Er_{NBC}=1.6\%$, with $\epsilon_s=90\%$ and, for S_2, $Er_B=1.1\%$, $Er_{NBC}=0.06\%$ with $\epsilon_s=30\%$.

$y_b=0.15x_b+(x_b-5)^2/2+0.125\sin t-0.4$, and S_2 where (x_b, y_b) is parametrized using $x_b/H=0.175\cos t+2.5$ and $y_b=0.3x_b/H+2(x_b/H-2.5)^2+0.125\sin t-0.4$.

To allow for comparison, a reference solution $p_M(x,y)$ is calculated using the finite element code MELINA.[33] The modal components $p_n(x)$ are deduced by interpolating $p_M(x,y)$ on a regular mesh and by projecting numerically onto the $\psi_n(y)$-basis. The scattered reference field $p^s_M(x,y)$ and the field $p^s_{NBC}(x,y)$ calculated from Eq. (12) [see also Eqs. (A3) and (A4)] are reported in Fig. 2, and the corresponding modal components $p_n(x)$ in Fig. 3. We have considered an incident plane wave of unity amplitude (for clarity of the curves of the modal components, the modal component of the incident wave e^{ik_Nx} is omitted). The maximum scattering amplitude are respectively 0.9 and 0.3, and NBC appears to be able to capture accurately the solution (here, $N_{mod}=10$ and $N_{it}=6$ have been considered).

D. Analytical expressions of the reflection and transmission coefficients

The first Born approximation leads to simple forms of the reflection and transmission coefficients, defined by

$$\begin{cases} p^1_n(x_s<x<0)=e^{ik_Nx}\delta_{nN}+R_{nN}e^{ik_nx} \\ p^1_n(x>L)=T_{nN}e^{ik_nx}, \end{cases} \tag{13}$$

by using $i=0$ in Eqs. (10) and (11):

$$\begin{aligned} R_{nN}&=\frac{(\rho/\tilde{\rho}-1)}{2ik_nH}\left[-k_nk_N\hat{C}_{nN}(k_N+k_n)\right. \\ &\quad\left.+\hat{D}_{nN}(k_N+k_n)\right]-\frac{k^2(B/\tilde{B}-1)}{2ik_nH}\hat{C}_{nN}(k_N+k_n), \\ T_{nN}&=\delta_{nN}+\frac{(\rho/\tilde{\rho}-1)}{2ik_nH}\left[k_nk_N\hat{C}_{nN}(k_N-k_n)\right. \\ &\quad\left.+\hat{D}_{nN}(k_N+k_n)\right]-\frac{k^2(B/\tilde{B}-1)}{2ik_nH}\hat{C}_{nN}(k_N-k_n), \end{aligned} \tag{14}$$

where $\hat{F}(q)\equiv\int_{\mathcal{C}_x}dx'e^{iqx'}F(x')$ is basically related to the Fourier transform of the inclusion shape for propagative modes.

E. Analytical solution in the case of small inclusion size compared to the waveguide height

We inspect in this section the simplifications that occur when considering small symmetrical inclusions, namely for inclusions of typical size $R\ll H$ (at this stage, no assumption about the kR-value is necessary). In that case, $a(x)=y_0-H\epsilon(x)$, $b(x)=y_0+H\epsilon(x)$, and $\epsilon(x)\sim\epsilon\equiv R/H\ll 1$. We get the following for C_{nN} and D_{nN}:

$$\begin{cases} C_{nN}(x)=2c_{nN}/k_N\ \epsilon(x)+O(\epsilon^2), & c_{nN}\equiv\alpha_{nN}\ k_NH\cos\dfrac{n\pi y_0}{H}\cos\dfrac{N\pi y_0}{H} \\ D_{nN}(x)=2k_nd_{nN}\ \epsilon(x)+O(\epsilon^2), & d_{nN}\equiv 2nN\dfrac{\pi^2}{k_NH}\sin\dfrac{n\pi y_0}{H}\sin\dfrac{N\pi y_0}{H}, \end{cases} \tag{15}$$

so that Eq. (2.13) becomes

$$\begin{cases} T_{nN}=\delta_{nN}+i\left[-(\rho/\tilde{\rho}-1)(d_{nN}+c_{nN})+k^2/(k_nk_N)\left(B/\tilde{B}-1\right)c_{nN}\right]\ I_{\mathcal{C}_x}(k_N-k_n) \\ R_{nN}=i\left[-(\rho/\tilde{\rho}-1)(d_{nN}-c_{nN})+k^2/(k_nk_N)\left(B/\tilde{B}-1\right)c_{nN}\right]\ I_{\mathcal{C}_x}(k_N+k_n) \end{cases} \tag{16}$$

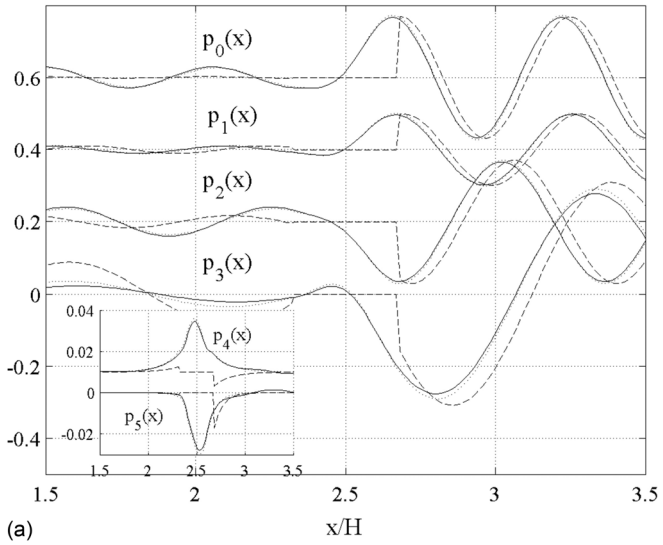

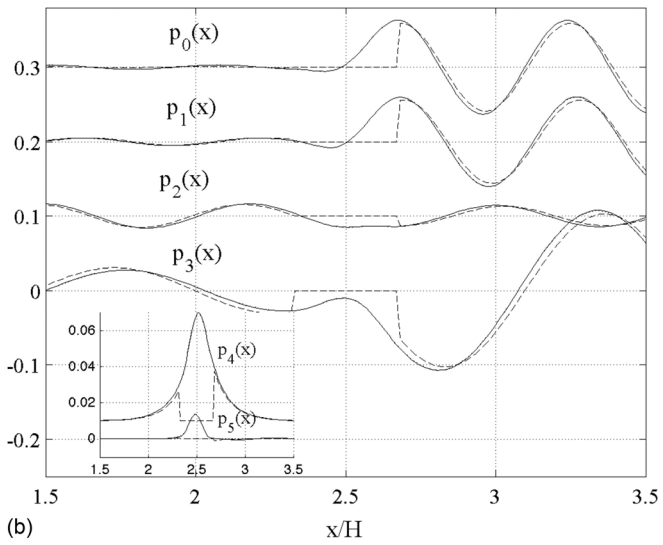

FIG. 3. Modal components $p_n(x)$ [the modal component $e^{ik_{xN}x}$, here for $N=0$, is omitted in $p_0(x)$] in the same cases as in Fig. 2. In solid line, $p^s_M(x,y)$, in dotted lines in the NBC calculations using Eq. (11) (almost indistinguishable with the solid line) and in dashed lines in the first Born approximation [Eq. (12)]. The curves are shifted from the zero mean for clarity.

with

$$I_{\mathcal{C}_x}(q) \equiv \frac{1}{H}\int_{\mathcal{C}_x} dx'\ \epsilon(x')e^{iqx'}. \tag{17}$$

The result is $O(\epsilon^3)$ if we assume that the size of the inclusion is of same order in both direction x and y (otherwise, $O(\epsilon^3)O(R_x/H)$ with R_x the typical size along x).

The dependence of T_{nN} and R_{nN} on the inclusion y_0-position is encapsulated in c_{nN} and d_{nN}, whereas the dependence on the x-position and on the shape of the inclusion is encapsulated in I_{Cx}. This latter integral can be evaluated for several inclusion shapes. As an example, we have, for a cylinder of radius R

$$I_{\mathcal{C}_x}(q) = \frac{\pi R^2}{H^2}\frac{J_1(qR)}{qR}e^{iqx_0}, \tag{18}$$

where J_n denotes the first kind Bessel function.

As other examples, the case of rectangular inclusions, of lateral extension $2R_x$ and of height $2R$ gives $I_{\mathcal{C}_x}(q) = 2(R\ R_xA/H^2)\mathrm{sinc}qR_x\ e^{iqx_0}$ or the case of a diamond shape, of lateral extension $2A$ and of height $2a$, corresponds to $I_{\mathcal{C}_x}(q) = aA/H^2\ \mathrm{sinc}^2(qA/2)e^{iqx0}$. Note that we have not assumed that the size of the inclusions is small with respect to the incident wavelength $2\pi/k_N$. If the case, the wave is not sensitive to the inclusion shape and

$$I_{\mathcal{C}_x}(q) = \frac{S}{2H^2}e^{iqx_0};$$

we get an additional simplification where S is the surface of the inclusion.

III. INSPECTION OF THE VALIDITY OF THE SCATTERED FIELD

In this section, we inspect the accuracies of the NBC and of our analytical expression (referred as B) in Eq. (16). The solution

$$p_M(x,y) = p^{inc}(x,y) + p^s(x,y), \tag{19}$$

calculated using the MELINA code is assumed to be the reference solution $p(x, y)$ and we measure the scattering strength, for an incident wave of amplitude unity by

$$\epsilon_s \equiv \max|p^s(x,y)|, \tag{20}$$

where the maximum value is calculated over the calculation domain. The errors are then defined as

$$Er_B \equiv \left|p^s_B - p^s\right|, \qquad Er_{NBC} \equiv \left|p^s_{NBC} - p^s\right|, \tag{21}$$

and $|X|$ refers to the mean value of X over the calculation domain. As previously reported, we expect the Born approximations to be valid for weak scattering, namely $\epsilon_s \ll 1$. Varying the parameters kR, $\tilde{\rho}/\rho$, and $\tilde{c}/c$, we will show in the following that

$$Er_B \simeq \epsilon_s^2 \tag{22}$$

or equivalently

$$p^s = \epsilon_s \rightarrow p = p^{inc} + p^s_B + \epsilon_s^2 \tag{23}$$

for $\epsilon_s < 1$ (up to values close to unity), meaning strong scattering regime. When this is the case, iterating the Born approximation P^s_{NBC} causes the solution to converge to p^s. If not $(\epsilon_s > 1)$, iterating the Born approximation causes the solution to diverge. The prediction of Eq. (16) has an additional assumption of small inclusion size compared with the height of the waveguide $2R/H \ll 1$, that is inspected varying $2R/H$.

A. Convergence of p_B, p_{NBC} varying N_{mod} (N_{it})

We show here the results obtained for the scattering of an incident plane wave (in mode 0) by a cylindrical inclusion (with, respectively, small and large $2R/H$ values) and a

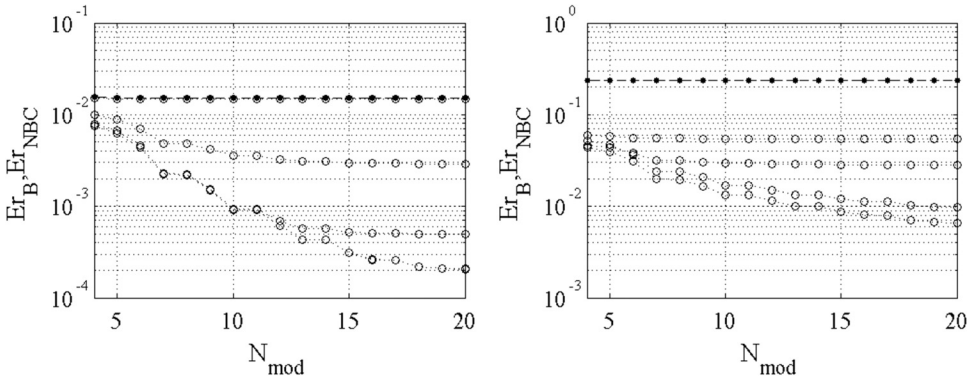

FIG. 4. Errors on p_B (closed symbols) and p_{NBC} (open symbols) as a function of N_{mod} in the case of the scattering by the cylinders C_1 (left) and C_2 (right). Decreasing Er_{NBC}-values at fixed N_{mod} correspond to $N_{it}=1, 2, 3, 6, 11$. Increasing further $N_{mod}>20$ and $N_{it}>11$ does not produce better convergence in these cases.

contrast in density (respectively, contrast in wavespeed) of 0.5. In the first case, the cylindrical inclusion C_1 has a small size ($kR=0.55$, $2R/H=0.1$) producing a scattered field of amplitude $\epsilon_s=21\%$. In the second case, the cylindrical inclusion C_2 has a large size ($kR=3.34$, $2R/H=0.6$), producing a scattered field of amplitude $\epsilon_s=110\%$. In both cases, we have $kH=11.12$, thus four propagative modes. Figure 4(a) shows the variation of the error Er_B as a function of the number of accounted modes and the variations of the error Er_{NBC} as a function of the number of modes for increasing $N_{it}=1$, 2, 3, 6, 11 iterations. We observe $Er_B \sim Er_{NBC}(N_{it}=1)\sim 1.5\%$ (close to $\epsilon_s^2=4\%$) with no significant variation on N_{mod}, starting from the four propagative modes and accounting for additional evanescent modes. Increasing N_{it} and N_{mod} causes p_{NBC} to converge to errors less than 0.1%. In the second case, our analytical prediction p_B is inaccurate, with an error of $\sim 25\%$, see Fig. 4(b). However, it appears that p_{NBC} has a significantly smaller error, even for $N_{it}=1$ ($Er_{NBC}=10\%$) and rapidly converges when increasing N_{it} and N_{mod} until less than 1%. In that case, the large R/H value is the source of the difference between Er_B and $Er_{NBC}(N_{it}=1)$, as the analytical prediction p_B is done for small R/H-values. Also, the large error is attributable to the high value of the scattered field, ϵ_s close to 1.

In these two situations, the main condition to make p_B and p_{NBC} accurate is the ϵ_s-value that clearly defined the validity condition of the Born approximation. This is inspected further varying the other parameters that define the scattering strength ϵ_s. Then, increasing R/H causes the analytical prediction p_B to be less and less precise [p_B is accurate up to $(R/H)^3$, a restriction that does not affect p_{NBC}].

B. Influence of the contrast in density or contrast in wavespeed

The contrasts in density and in wavespeed are two parameters that define the scattering strength of the inclusion. Their influences on the accuracy of p_B (close symbols) and p_{NBC} (open symbols for $N_{it}=1$ and 6) are illustrated on the Fig. 5, together with the amplitude ϵ_s of the scattered field. In the range of explored contrasts ($\tilde{c}/c$, $\tilde{\rho}/\rho$ varying between 0.5 and 10 for an inclusion size $kR=0.56$), the scattered field has an amplitude ϵ_s varying between 10^{-2} to a value close to 1. Within this range, the corresponding accuracy of our analytical prediction p_B roughly behaves like ϵ_s^2 as expected. As previously reported, this produces a significant error (up to 20%) for ϵ_s close to 1. We also observe that p_{NBC} converges when increasing N_{it}, for these $\epsilon_s \lesssim 1$.

C. Influence of the inclusion size and wavenumber

As qualitatively seen in Sec. III A, considering the influence of the inclusion size has two aspects: Basically, increasing R produces an increase in the scattering strength. On the other hand, the analytical prediction p_B has an additional assumption of small R/H-values.

We report in Fig. 6(a) the errors Er_B (close symbols with dashed line) and Er_{NBC} (open symbols with: dashed line for $N_{it}=1$ and dotted line for $N_{it}=6$), together with the value of the scattered field ϵ_s (solid line) as a function of kR. Here, the R/H value is constant and increasing kR (by increasing k in a fixed geometry) produces an increase in the scattering strength of the inclusion [typically $p^s=\epsilon_s \propto (kR)$ for a fixed geometry]. In the presented range of kR-values, the scattered amplitudes ϵ_s remain smaller than 20% and

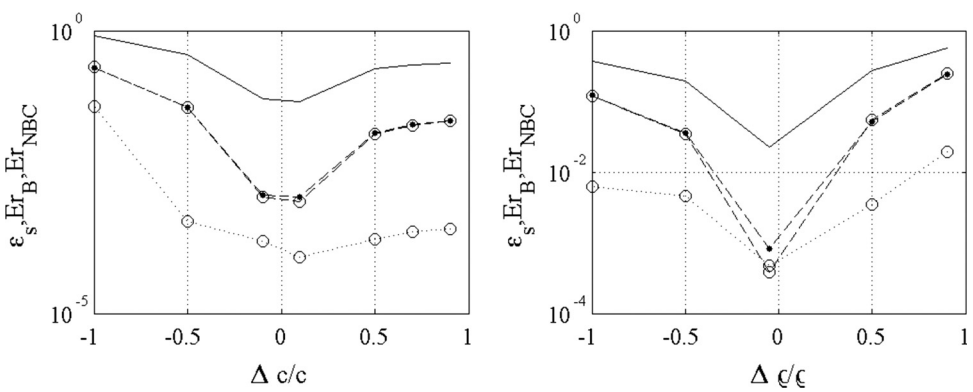

FIG. 5. Errors as a function of the contrast in (left) wavespeed $\Delta c/\tilde{c}\equiv 1-c/\tilde{c}$ and (right) density $\Delta\rho/\tilde{\rho}\equiv 1-\rho/\tilde{\rho}$. The solid line shows the amplitude of the scattered field ϵ_s, the errors are Er_B (closed symbols with a dashed line) and Er_{NBC} (open symbols with a dashed line for $N_{it}=1$ and a dotted line for $N_{it}=6$). Calculations are for an inclusion located at ($x_0/H=2.5$, $y_0/H=0.35$) for an incident wave in mode 0 with $kH=11.12$, $2R/H=0.1$.

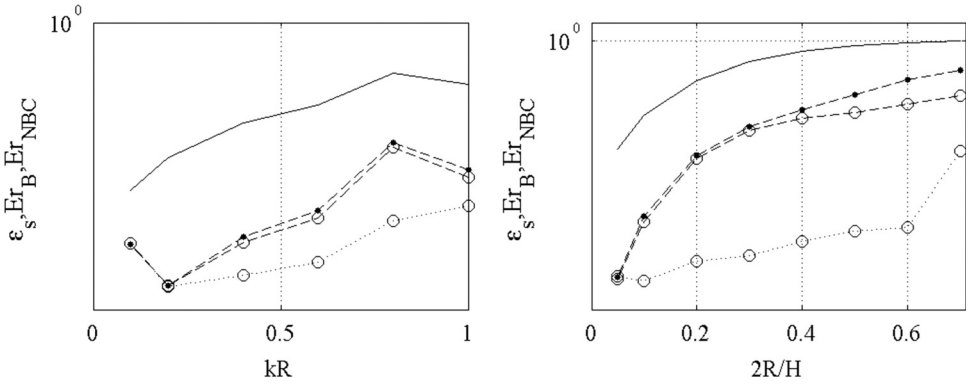

FIG. 6. Errors as a function of the size of the inclusion kR or $2R/H$. The solid line shows the amplitude of the scattered field ϵ_s, and the errors are Er_B (closed symbols with a dashed line) and Er_{NBC} (open symbols with a dashed line for $N_{it}=1$ and a dotted line for $N_{it}=6$). The errors are calculated for an inclusion located at $(x_0/H=2.5,\ y_0/H=0.35)$, with no contrast in density and a contrast in wavespeed $c/\tilde{c}=0.9$, for an incident plane wave (mode 0) with (left) $2R/H=0.1$ varying kR and (right) $kH=11.12$ varying $2R/H$.

we observe the same behaviors than when varying the contrasts in density and in wavespeed (Fig. 5): $Er_B \sim Er_{NBC}(N_{it}=1) \sim \epsilon_s^2$ and the p_{NBC} converges when increasing N_{it}.

Figure 6(b) shows the same quantities as Fig. 6(a) but here, the size of the inclusion R has been increased, for fixed k and H, producing both a change in kR and in R/H. With $\epsilon_s < 1$, the same behavior of p_{NBC} is observed, with $Er_{NBC}(N_{it}=1) \sim \epsilon_s^2$ and a convergence when increasing N_{it}. More importantly, for large R/H-values (here $2R/H > 0.5$), the analytical estimate p_B presents a larger error that $p_{NBC}(N_{it}=1)$, due to the assumption of small R/H-value used in the former case: namely $Er_{NBC} \simeq \epsilon_s^2$, whereas $Er_B \simeq \epsilon_s^2(1+O(R^3/H^3))$.

D. Limit of validity of the Born approach

As previously said, p_B and p_{NBC} are expected to be accurate for weak scattering and we have illustrated that in the practice, even configurations leading to scattering strengths ϵ_s close to 1 are reasonably described by our approximations. Figure 7 illustrates the limit of validity of our Born approach: The same calculations as in Fig. 6(b) have been conducted but with an higher contrast in wavespeed $c/\tilde{c}=0.5$, producing a significantly higher scattering, with ϵ_s from a few percent to about 300%.

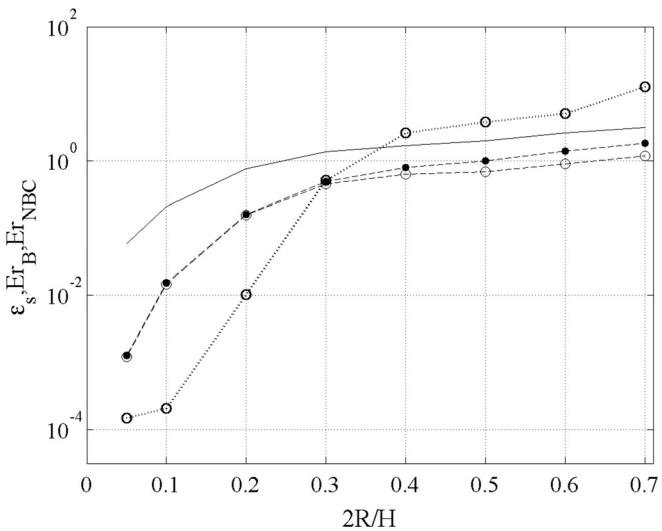

FIG. 7. Errors as a function of the size of $2R/H$. Same representation as in Fig. 6 and the errors are calculated for the same configuration, but with an higher contrast in wavespeed $c/\tilde{c}=0.5$.

For small ϵ_s-values, until say close to 1 ($2R/H < 0.3$), the same trend as previously is observed: $Er_B \sim Er_{NBC}(N_{it}=1) \sim \epsilon_s^2$ and iterating the Born approximation causes p_{NBC} to converge. But we also see that for ϵ_s-values larger than unity, the large error in Er_{NBC} ($N_{it}=1$), typically of order 100% causes the solution to diverge when increasing N_{it}.

Similar divergence (not shown) has been observed for large scattering due to high contrasts in density or wavespeed or due to large kR-values. In conclusion, the only pertinent parameter for the validity of the Born approximation is the scattering strength and it turns out that it is valid even for strong scattering (namely for amplitude of the scattered field close to the amplitude of the incident wave).

IV. ANALYTICAL SOLUTIONS FOR PERIODICALLY OR RANDOMLY DISTRIBUTED INCLUSIONS

In this section, we inspect the analytical solution $p_B(x, y)$ for particular distributions of inclusions: Periodic and random. In both cases, the solution is compared to results concerning the scattering by inclusions in the unbounded free space in the low frequency regime. For periodically distributed inclusions, particular modes of the waveguides are shown to be excited, and the equivalence with the usual grating law is exhibited. Also, the Bragg scattering is recovered. For randomly distributed inclusions, the reflection and transmission coefficients are found to account for the shape of the inclusion, particularly relevant in the high frequency regime.

A. Scattering by inclusions periodically distributed, analogy with an infinite array of inclusions

1. Scattering by periodically distributed inclusions

We considered $N_x \times N_y$ scatterers periodically distributed in $[0; L] \times [0, H]$ with

$$x_{0m} = ml, \quad m = 0, \ldots, N_x - 1, \quad l = L/N_x,$$
$$y_{0p} = h/2 + ph, \quad p = 0, \ldots, N_y - 1, \quad h = H/N_y. \quad (24)$$

The sum over the N_x vertical sets of inclusions is accounted for in $\mathcal{C}_x = \cup_m[x_{0m} - D; x_{0m} + D]$, whereas the sum over the N_y vertical inclusions appears in c_{nN}, d_{nN} : For each $x \in C_x$, a succession of N_y $[a_p(x), b_p(x)]$ has to be accounted for thanks to the transformations $c_{nN} \to Sc_{nN}$ and $d_{nN} \to Sd_{nN}$ in Eq. (16) with

$$Sc_{nN} = \sum_{p=0}^{N_y-1} c_{nN} \equiv \alpha_{nN} k_N H \frac{H}{2h}\Big[(-1)^{j_1}\delta_{n\left(N+2j_1N_y\right)} + (-1)^{j_2}\delta_{n\left(-N+2j_2N_y\right)}\Big],$$
$$Sd_{nN} \equiv \sum_{p=0}^{N_y-1} d_{nN} = nN\frac{\pi^2}{2k_n h}\Big[(-1)^{j_1}\delta_{n\left(N+2j_1N_y\right)} + (-1)^{j_2}\delta_{n\left(-N+2j_2N_y\right)}\Big], \tag{25}$$

where j_1 and j_2 are integers. Using Eq. (11), the solution can be written as

$$p_n^1(x) = e^{ik_N x}\delta_{nN} - i(\rho/\tilde{\rho}-1)\frac{1}{H}\sum_{m=0}^{N_x-1}\int_{md-D}^{md+D} dx'\ [\mathrm{sign}(x-x')Sc_{nN} + Sd_{nN}]\epsilon(x')e^{ik_n|x-x'|+ik_N x'}$$
$$+ ik^2\left(B/\tilde{B}-1\right)\frac{1}{k_N k_n H}Sc_{nN}\sum_{m=0}^{N_x-1}\int_{md-D}^{md+D} dx'\ e^{ik_n|x-x'|+ik_N x'}\epsilon(x') + O\left(\epsilon^3\right). \tag{26}$$

It is now sufficient to use

$$I_{\mathcal{C}x}(q) = \frac{1}{H}\sum_{m=0}^{N_x-1}\int_{md-D}^{md+D} dx'\ e^{iqx'}\epsilon(x') = \frac{1-e^{iqL}}{1-e^{iqL}}I_{\mathcal{C}x0}(q), \tag{27}$$

where $\mathcal{C}_{x0}$ is the interval of the first inclusion along the x-axis $[-D;\ +D]$ [we also consider $(1-e^{iqL})/(1-e^{iql}) = L/l$ for $q=0$], to get the reflection and transmission coefficients by a periodic set of inclusions,

$$\begin{cases} T_{nN}^{perio} = \delta_{nN} + i\left[-(\rho/\tilde{\rho}-1)(Sd_{nN}+Sc_{nN}) + k^2/(k_n k_N)\left(B/\tilde{B}-1\right)Sc_{nN}\right]\dfrac{1-e^{i(k_N-k_n)L}}{1-e^{i(k_N-k_n)l}}I_{\mathcal{C}x0}(k_N-K_n) \\ R_{nN}^{perio} = i\left[-(\rho/\tilde{\rho}-1)(Sd_{nN}-Sc_{nN}) + k^2/(k_n k_N)\left(B/\tilde{B}-1\right)Sc_{nN}\right]\dfrac{1-e^{i(k_N+k_n)L}}{1-e^{i(k_N+k_n)l}}I_{\mathcal{C}x0}(k_N-K_n). \end{cases} \tag{28}$$

A typical example is given in the following for an incident wave in mode 1. Figure 8 shows the scattered fields p_M^s and p_B^s and the corresponding modal components p_n (in the presented case, for an incident wave in mode 1, only odd modes are excited).

The transmission coefficients T_{n1} deduced from MELINA calculation for even modes are of order 10^{-3} (our prediction is zero for these modes). The transmission coefficients for odd modes are $T_{11}^M = -1.24i$ and $T_{31}^M = 0.20 + 0.26i$ in good agreement with our predictions from Eq. (28): $T_{11}^M = -1.29i$ and $T_{31} = 0.24 + 0.25i$.

2. Analogy with an infinite array of inclusions, grating law and Wood's anomalies

For an infinite array of h-spaced scatterers, the classical grating criterion gives the directions θ_n in which constructive interferences are observed:

$$kh\sin\theta_m = kh\sin\theta + 2m\pi, \tag{29}$$

where θ is the angle of the incident wave (measured from the x-axis). The symmetry of the problem and the Neumann boundary conditions on the waveguide walls makes the configuration analogous to an infinite array of inclusions for an incident wave formed of the superposition of two waves with incidences $\pm\theta$ satisfying $k\sin\theta = N\pi/h$. Note that general incidences can be treated in the context of Rayleigh Bloch waves leading to pseudo-periodic boundary conditions (instead of Neumann boundary conditions).[34] Here, the angle θ_m has to be related to an order n of a propagating mode, namely $n\pi \equiv kh\sin\theta_m$. The grating criterion, Eq. (29), gives that n and N have the same parity, $n = N + 2m$, in agreement with the selection of propagating modes in Eq. (25) [with $N_y = 1$ in Eq. (25)]. Obviously, the selection of evanescent modes in Eq. (25) is not accounted in the grating criterion (then $|\sin\theta_m| > 1$), which considers only the far field.

Finally, it appears that the representation in Eq. (26) breaks down if $k_n = 0$ ($\cos\theta_m = 0$), a singularity known as Wood's (or Rayleigh) anomaly.[35,36] It corresponds to a spectral order emerging at grazing angle, or to a mode passing a cutoff frequency. This has been analyzed in details in the case of sound hard and sound soft cylinders in Ref. 37.

3. The case of an incident plane wave, comparison with Twersky's prediction

Although our prediction enables us to consider an incident wave forming an angle θ with the array of inclusions, we consider for simplicity the case of an incident plane wave and we consider a grating with $N_y = 1$. In that case, the equations in Eq. (28) simplify to

$$\begin{cases} T_{n0}^{perio} = \delta_{n0} + i\alpha_{n0}\dfrac{kS}{2H}\left[-(\rho/\tilde{\rho}-1)+k/k_n\left(B/\tilde{B}-1\right)\right]\cos\dfrac{n\pi}{2}\mathcal{S}((k-k_n)R) \\ R_{n0}^{perio} = i\alpha_{n0}\dfrac{kS}{2H}\left[(\rho/\tilde{\rho}-1)+k/k_n\left(B/\tilde{B}-1\right)\right]\cos\dfrac{n\pi}{2}\mathcal{S}((k-k_n)R) \end{cases} \tag{30}$$

with $S=\pi R^2$ the surface of the inclusion and

$$\mathcal{S}(qR) \equiv \frac{2J_1(qR)}{qR} \tag{31}$$

a factor depending on the shape of the inclusion (here given for a cylindrical shape). These predictions are expected to be valid for small R/H-values, but they are valid even in the high frequency regime kR, $kH>1$, where several propagative modes exist, corresponding to several orders of interference as previously commented. Typical scattered fields are presented in Fig. 9(a) in the low frequency ($kR=0.7$, $kH=14$, thus 4 propagative modes) and in the high frequency ($kR=1.8$, $kH=36$, thus 11 propagative modes) regimes. Figure 9(b) shows the corresponding reflection coefficients as a function of the n-value. As expected from the symmetry of the system, only the even modes are excited. This condition is encapsulated in the term $\cos n\pi/2$ in Eq. (30). It also corresponds to the grating criterion Eq. (29), $k=2m\pi/H$ (and $n=2m$). We observe a good agreement between direct calculation of R_{n0} (close symbols) and our analytical prediction [open symbols, from Eq. (30)].

Incidentally, in the high frequency regime ($kH=36$), where the field pattern can be analyzed in terms of ray trajectory, the observed pattern (here in reflection) clearly corresponds to the superposition of two plane waves forming an angle of, respectively, $\pm\theta$, with $\tan\theta\sim 1.8$. This θ-value corresponds to the mode $n=10$, using $\tan\theta=k_y/k_n$, [$k_y=n\pi/H$, $k_n=\sqrt{k^2-(n\pi/H)^2}$]. Here, the kH-value is close to the cutoff frequency of the mode 10 at $k_cH=31.4$, and we have seen that a mode is resonant at its cutoff frequency (Wood's anomaly).

In Fig. 10, we reported the variation of $|R_{n0}|$ varying the frequency kR (same configuration as in Fig. 9 has been considered). Results deduced from MELINA calculations and our estimate Eq. (30) (solid line) are in good agreement (the errors Er_B in the whole range of kR-values is less than 8%). Figure 10 also illustrates the pertinence of the shape factor $\mathcal{S}$

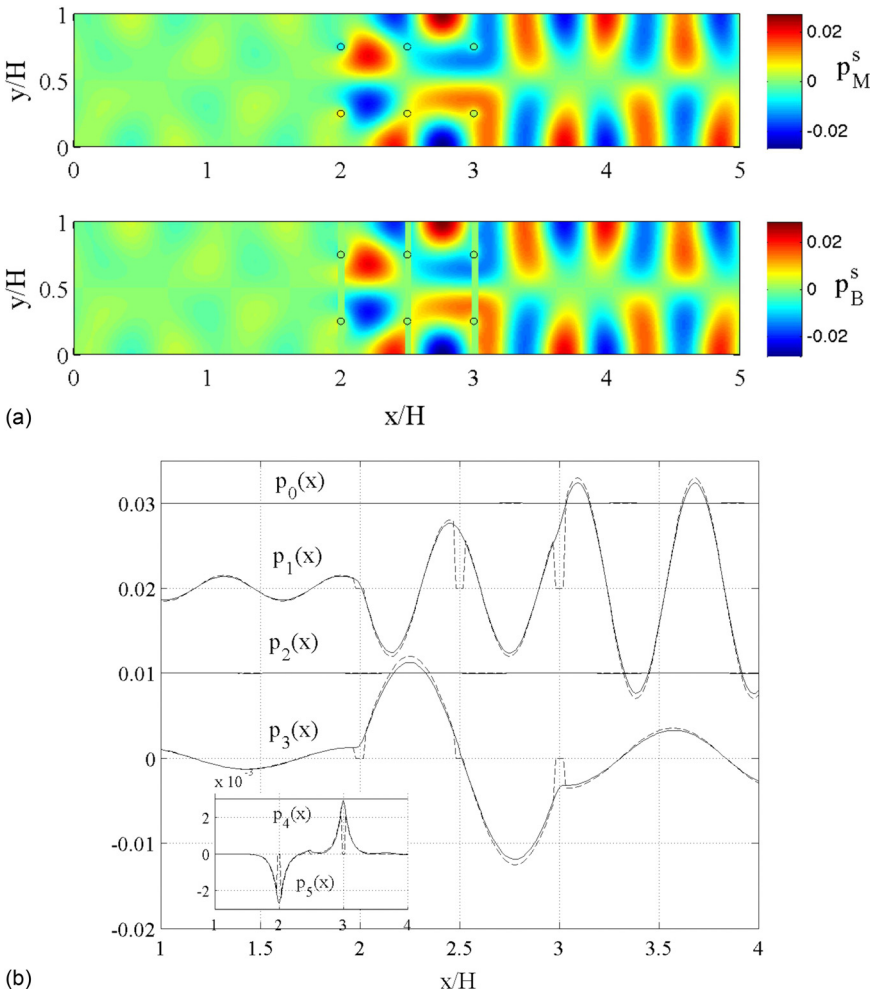

FIG. 8. (Color online) Scattering by a periodic set of scatterers [$x_{0p}/H=(2,\ 2.5,\ 3)$, $y_{0m}/H=(0.25,\ 0.75)$] for the mode 1 incident ($k=5.56$, $R=0.05$, $c/\tilde{c}=0.9$, $\rho=\tilde{\rho}$). (a) Scattered field p^s_M, on the bottom p^s_B using Eqs. (4.5). The error is $Er_B=6\%$. (b) $p_n(x)$ for $n=0,.,6$, solid lines correspond to the results obtained with MELINA code, dashed–dotted line to the solution using Eq. (4.5). Only odd modes are expected to be nonvanishing from Eq. (4.2).

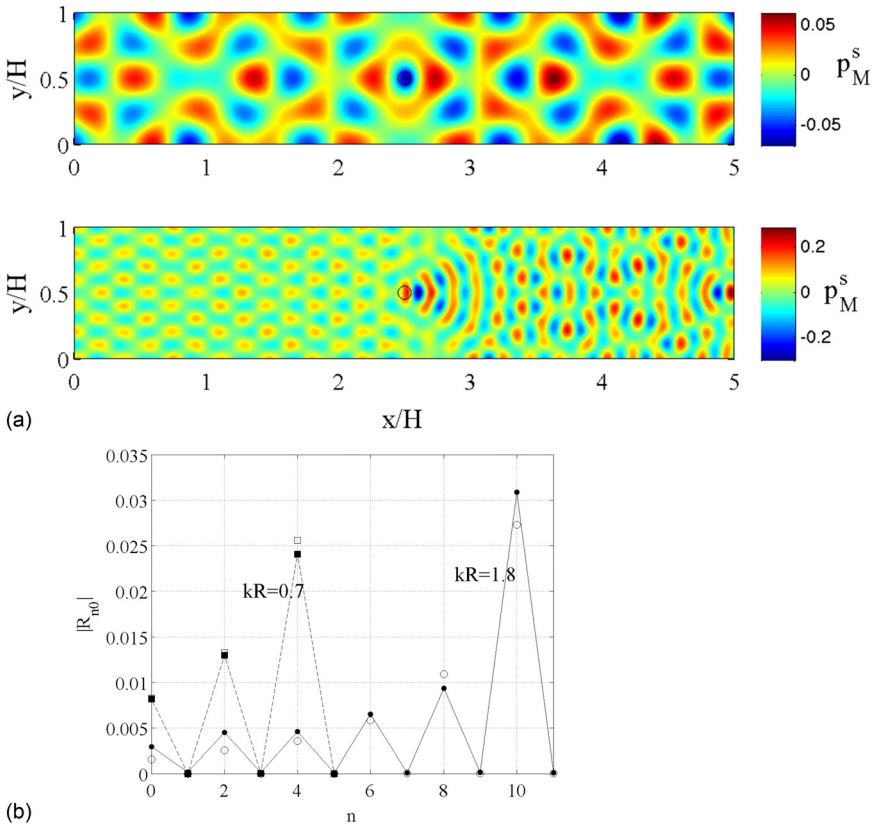

FIG. 9. (Color online) (a) Scattered fields $p^s_M(x,y)$ by an infinite array of cylindrical inclusions H-spaced and (b) corresponding reflection coefficients $|R_{n0}|$ as a function of n. The inclusion has a contrast in wavespeed $c/\tilde{c}=0.9$ and $2R/H=0.1$ (no contrast in density). (Top) $kR=0.7$ and (bottom) $kR=1.8$.

in Eq. (30) when increasing the frequency (dotted line give the result when omitting this factor).

It is of interest to compare our result with the prediction given by Twersky[38,39] in the low frequency regime, namely the limit $kR, kH \to 0$. With $f(\theta)$ the scattering function of a single inclusion in free space [here defined as $p^s(\mathbf{r}) \to f(\theta)\sqrt{2/\pi kr}e^{ikr-i\pi/4}$ in the far field], he found (a clear derivation can be found in Eq. (3.1.a,b) of Ref. 40],

$$\begin{cases} T^T = 1+\dfrac{4if(0)}{2ikH} = 1+i\dfrac{kS}{2H}\left[-2\dfrac{\rho-\tilde{\rho}}{\rho+\tilde{\rho}}+\left(B/\tilde{B}-1\right)\right] \\ R^T = \dfrac{4if(\pi)}{2ikH} \quad = i\dfrac{kS}{2H}\left[2\dfrac{\rho-\tilde{\rho}}{\rho+\tilde{\rho}}+\left(B/\tilde{B}-1\right)\right], \end{cases} \tag{32}$$

where we used, for cylindrical inclusions $4\mathrm{i}\, f(\theta) = \pi(kR)^2\left[1-B/\tilde{B}\right] + 2\pi(kR)^2(\rho-\tilde{\rho})/(\rho+\tilde{\rho})\cos\theta$.

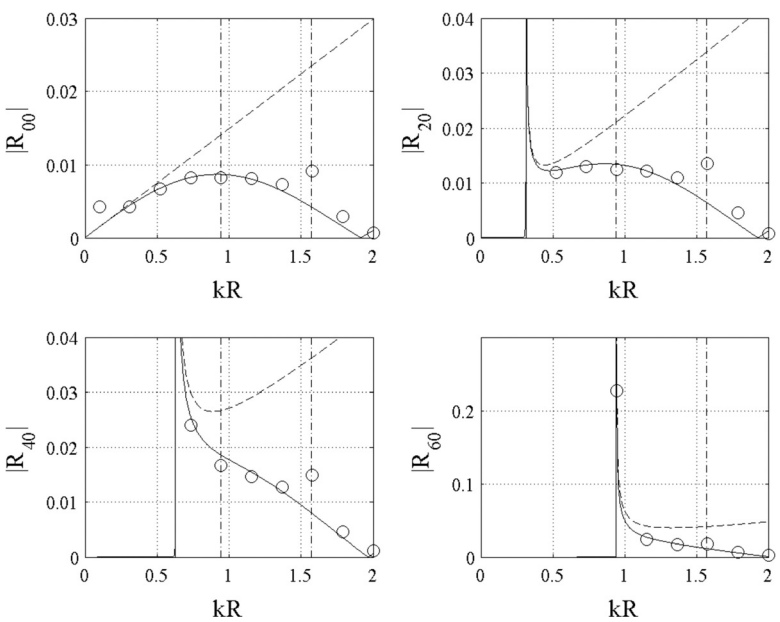

FIG. 10. Reflection coefficients $|R_{n0}|$ as a function of the frequency kR (same configuration as in Fig. 9 has been considered). Open circles from MELINA calculations, solid lines from our prediction Eq. (4.7), and dashed line using Eq. (4.7) but omitting the factor of shape S. Vertical lines indicate some cutoff frequencies from $kH=2\pi$ ($kR=0.31$) to $kH=10\pi$ ($kR=1.57$).

This coincides with the plane wave approximation, where our estimates in Eq. (30) simplify in

$$\begin{cases} T_{00}^{perio} = 1 + i\dfrac{kS}{2H}\left[-(\rho/\tilde{\rho}-1) + \left(B/\tilde{B}-1\right)\right] \\ R_{00}^{perio} = i\dfrac{kS}{2H}\left[(\rho/\tilde{\rho}-1) + \left(B/\tilde{B}-1\right)\right] \quad \mathcal{S}(2kR). \end{cases} \tag{33}$$

There are obviously differences between the predictions: (1) Our predictions account for the shape of the inclusion and for the frequency regime through the term $\mathcal{S}(2kR)$ and (2) the dependence in the contrast in density in Twersky's prediction differs from ours, except for small contrasts. These two discrepancies are inspected in the following.

We calculated from MELINA results the reflection coefficient in the low frequency regime ($kR=0.15$, $kH=3$) for various contrasts in density and for various contrasts in wavespeed. The results are reported in Fig. 11. In the considered configuration, $\mathcal{S}(2kR)=0.99$ is irrelevant and our estimate on R_{00}^{perio} differs from R_T only on the dependence on the contrast in density. Both predictions appear to be accurate when varying the contrast in wavespeed. When varying the contrast in density, our estimate (solid line, MELINA results are given by open circles) appears to be less accurate than Twersky's (dotted line). This means that the first Born approximation gives the leading order contribution $\rho/\tilde{\rho}$. Note that this has already been observed for the scattering of spheres in free space.[25] Then, iterating the NBC (star symbols in Fig. 11) recovers the dependence $2(\rho-\tilde{\rho})/(\rho+\tilde{\rho})$ that is approximated by $(\rho/\tilde{\rho}-1)$ in the first iteration. It follows a significant limitation of our analytical prediction unable to account for sound hard inclusions. We conclude that the first Born estimate is less accurate in the low frequency regime than other perturbative approximations (a conclusion already observed in Ref. 25) and attaining better accuracy requires to iterate NBC. On the other hand, it allows us to go beyond the low frequency regime, and to account for the shape of the inclusions. Further research is needed to inspect that possibility.

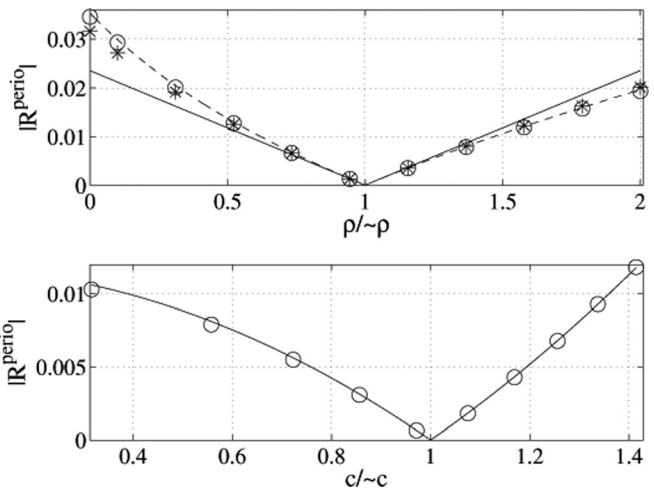

FIG. 11. Reflection coefficient as a function of the contrast in density $\rho/\tilde{\rho}$ and as a function of the contrast in wavespeed $c/\tilde{c}$ in the low frequency regime ($kR=0.15$, $kH=3$). Open circles, deduced from MELINA calculations (the point at $\rho/\tilde{\rho}=0$ has been obtained by applying Neumann boundary conditions at the inclusion boundary). Solid lines from our estimate in Eq. (33) and dotted lines from Twersky's estimate Eq. (32). Star symbols show the reflection coefficient when using the results of NBC with $N_{it}=10$.

B. Random distribution of inclusions

1. The case of randomly distributed inclusions in a waveguide

The case of a random distribution of N_s small inclusions occupying the space $x_i \in [0,L]$, $y_i \in [0,H]$, $i=1,\ldots,N_s$ is straightforward considering the linearity of Eq. (13). We have

$$\begin{cases} p_n^1(x_s < x < 0) = e^{ik_N x}\delta_{nN} + \displaystyle\sum_{i=1}^{N_s} R_{nN}(x_i,y_i)e^{-ik_n x} \\ p_n^1(x > L) = \displaystyle\sum_{i=1}^{N_s} T_n N(x_i,y_i)e^{ik_n x} \end{cases} \tag{34}$$

with

$$\begin{cases} T_{nN}(x_i,y_i) = \delta_{nN} + i\left[-(\rho/\tilde{\rho}-1)(d_{nN}(y_i)+c_{nN}(y_i)) + k^2/(k_n k_N)\left(B/\tilde{B}-1\right)c_{nN}(y_i)\right] \quad I_{\mathcal{C}x_i}(k_N-k_n) \\ R_{nN}(x_i,y_i) = i\left[-(\rho/\tilde{\rho}-1)(d_{nN}(y_i)-c_{nN}(y_i)) + k^2/(k_n k_N)\left(B/\tilde{B}-1\right)c_{nN}(y_i)\right] \quad I_{\mathcal{C}x_i}(k_N+k_n), \end{cases} \tag{35}$$

and

$$I_{\mathcal{C}_{x_i}}(q) \equiv \frac{1}{H}\int_{\mathcal{C}_{x_i}} dx' \epsilon(x') e^{iqx'}, \tag{36}$$

The mean field is obtained by averaging over all realizations of disorder, and if we assume no correlations between scatterers

$$\langle\cdot\rangle \equiv \frac{1}{H^{N_s}}\frac{1}{L^{N_s}}\int dx_1\cdots dx_{N_s}\int dy_1\cdots dy_{N_s}. \tag{37}$$

The average over the x_i concerns $I_{\mathcal{C}_x}$ only and the average over the y_i concerns c_{nN} and d_{nN}. We get

$$\begin{cases} T_{NN}^{rand} = 1 + \dfrac{i\varphi}{2}\left[(k/k_N)^2\left(B/\tilde{B}-1\right) - (\rho/\tilde{\rho}-1)\left(1+(N\pi)^2/(k_N H)^2\right)\right]k_N L \\ R_{NN}^{rand} = -\dfrac{\varphi}{4}\left[\left(B/\tilde{B}-1\right)(k/k_N)^2 + (\rho/\tilde{\rho}-1)\left(1-(N\pi)^2/(k_N H)^2\right)\right]\left(1-e^{2ik_N L}\right)\mathcal{S}(2k_N\, R) \end{cases} \tag{38}$$

and $R_{nN}^{rand} = T_{nN}^{rand} = 0$ if $n \neq N$. We have defined $\varphi \equiv N_s S/LH$ the volume fraction of the inclusions.

Some remarks can be made at this stage: First, no mode conversion occurs, a result that has been already observed for hard inclusions from direct numerical calculations,[41] also observed in different context.[42,43] The dependence of T_{NN}^{rand} on the length L of the slab containing the inclusions is linear, a consequence of the linearity of our equation in the single scattering approximation, which causes the prediction on the transmission unreliable for large L. The limit of T_{NN}^{rand} for a large slab is less problematic: Including a small attenuation in the host medium that produces a small imaginary part in k_N, and the limit $L \to \infty$ becomes possible [namely $e^{2ik_N L}$ vanishes in Eq. (38)]. This limit will be inspected in the following section.

Numerical experiments to inspect the characteristics of effective media is quite difficult and only few attempts have been made.[41,44] It is out of the scope of the present paper to exhaustively study these characteristics as a function of the multiple parameters of the problem. We give a preliminary result concerning a unique configuration. Inclusions with $kR = 0.9$, $2R/H = 0.1$ are randomly distributed in a slab of length $L/H = 3$, the inclusion filling fraction is $\varphi = 10\%$. A typical realization of this disordered configuration is shown in Fig. 12, where the solutions p_M and p_B appear to be in good agreement, with an error $Er_B = 4\%$ [the modal components are also compared in Fig. 12(b)]. Here, p_B is calculated by summing the fields for each inclusion [Eqs. (13)–(17)], which produces an error as only the field reflected and transmitted by an inclusion is available analytically.

Averaging over several realizations of the disorder is expected to produce a coherent effective wave. In free space, an usual modelization of the resulting coherent field is expressed as $\langle p\rangle(x,y) \propto e^{iKx}$, where K has a real part that encapsulates the change in the wave speed due to the presence of the inclusions and an imaginary part due to the destructive interferences produced in the average process. The study of the validity of such modelization for guided propagation and the links between effective propagation in free space and effective guided propagation will be the subject of future works. Here, we propose only to test the validity of the transmission and reflection coefficients.

Figure 13 shows the mean scattered field $\langle p_M^s\rangle(x,y)$ obtained using MELINA code after 1000 realizations of the disorder (the disorder corresponds here to the random positions of the inclusions, otherwise considered identical in size and contrast). The total field $\langle p\rangle = p^0 + \langle p_M^s\rangle$ is not reported because the mean scattered field, with 20% in amplitude with respect to the incident wave, is too weak to produce a visible change (only the incident plane wave is visible). Let us however stress that the scattered mean field has an increasing amplitude when it "propagates" in the waveguide, a fact that is not intuitive, whereas the total mean field has a decreasing amplitude as expected, because of destructive interferences between p^0 and $\langle p^s\rangle$.

Inspecting this effective mean field gives the following conclusions:

(i) Figure 13(b) shows the modal components $\langle p_n\rangle(x)$ of $\langle p_M^s\rangle(x)$ for $n = 1$–4, to be compared with the modal components obtained for one realization [Fig. 12(b)]. In agreement with our prediction, the average causes the mode conversions to vanish and only mode 0 survives. Numerically, the amplitudes of the higher modes decrease in the average process and their maximum value after a finite number of averages can be used to define the limit of resolution in $\langle p_M^s\rangle$. Here, with 1000 averages, the maximum amplitude is observed for $n = 1$ and equals 0.02 (2% of the total mean field for a mode 0 corresponding to about 20% of the total mean field).

(ii) The transmission coefficient T_{00}^{rand} can be deduced from $\langle p_0\rangle(x/H > 4) = T_{00}^{rand} e^{ikx}$ (in each configuration, the inclusions are contained in the slab $x/H \in [1;4]$): we get $T_{00}^{rand} = 1.04 - 0.255\,i$, in

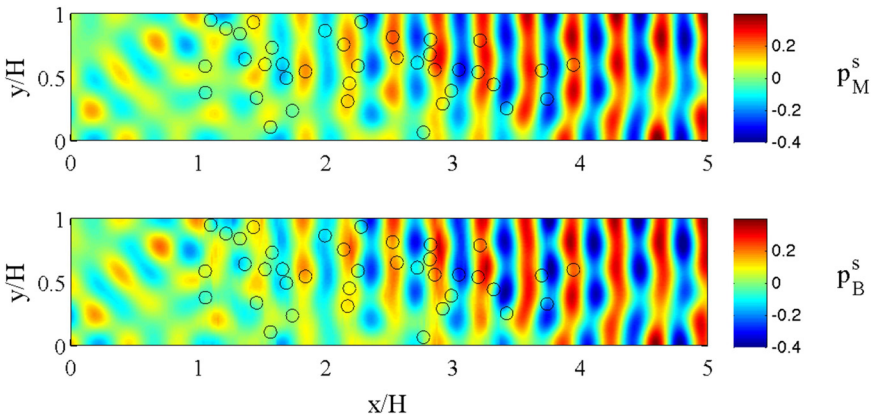

FIG. 12. (Color online) (a) Scattered field calculated with MELINA p_M^s and p_B^s (resulting error is $Er_B = 4\%$) and (b) corresponding modal components $p_n(x)$ for $n = 0$–3; solid line calculated from MELINA p_M^s and dotted line p_B,n. All the inclusions (here, 38 inclusions) have the same characteristics ($2R/H = 0.1$, $\rho/\tilde{\rho} = 1$, $c/\tilde{c} = 0.95$) and are located randomly between $x/H = 1$ and $x/H = 4$ with a filling fraction $\phi = 10\%$. The incident wave is a plane wave (mode 0) with $kR = 0.9$.

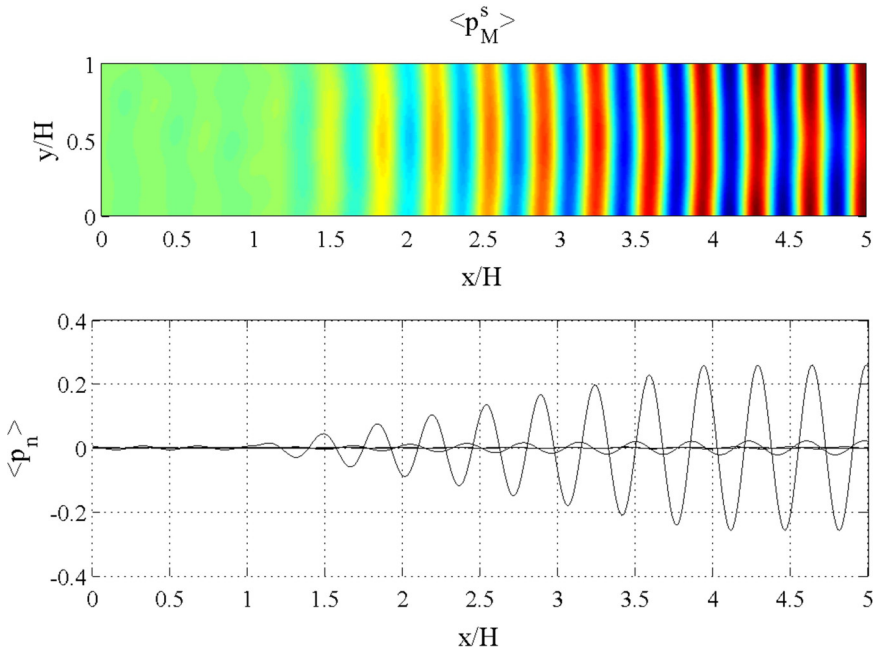

FIG. 13. (Color online) (Top) Mean scattered field $\langle p_M^s \rangle(x,y)$ obtained after averaging 1000 configurations of the randomly located inclusions. (Bottom) Corresponding mean modal components $\langle p_n \rangle(x)$ for $n=0$–3. For each realization of the disorder, the characteristics of the inclusions (size and contrasts) are the same as in Fig. 12 but the positions change.

reasonable agreement with our estimate Eq. (38) $T_{00}^{rand} = 1 - 0.263\,i$ (the error bar being 0.02 as previously discussed). The reflection coefficient can be deduced from $\langle p_0 \rangle(x/H < 1) = R_{00}^{rand} e^{-ikx}$. Numerically, we find a value of order 10^{-3} (our prediction gives $R_{00}^{rand} = 0.001 - 0.0015\,i$), but the values cannot be compared quantitatively because they are well below the resolution.

2. The case of a single interface, comparison with unbounded effective propagation

Our result concerns the reflection and transmission coefficients through a slab of randomly located inclusions in a waveguide. As previously said, this should allow us to deduce the characteristics of the guided effective wave, if it makes sense. Also, comparisons with results available for unbounded effective propagation make sense: Does a finite slab of randomly located inclusions behave as an unbounded random distribution? To answer this question, more precise and systematic numerical experiments are needed and this will be the subject of future works. However, a hint of how both guided and unbounded situations compare is the case of a unique interface between the free space and the effective medium. In that case, there is a prediction for the reflection coefficient at the interface in the low frequency regime[45–47] (small cylindrical inclusions with $kR \ll 1$), R^M [Eq. (2) in Ref. 47],

$$R^M = i\varphi \frac{f(\pi)}{k^2 S} = -\frac{\varphi}{4}\left[\left(B/\tilde{B} - 1\right) + 2\frac{\rho - \tilde{\rho}}{\rho + \tilde{\rho}}\right], \qquad (39)$$

where f is, as in the periodic case, the scattering function. Considering the limit $L \to \infty$ in our Eq. (38), we get

$$R_{00}^{rand} = -\frac{\varphi}{4}\left[\left(B/\tilde{B} - 1\right) + (\rho/\tilde{\rho} - 1)\right]\mathcal{S}(2kR), \qquad (40)$$

where we have used the artifact of a small attenuation in the host medium to take the limit $e^{ikL} \to 0$. Considering the limit $ka \to 0$ (as assumed in Refs. 46 and 47) and $\rho \sim \tilde{\rho}$ causes the two results to coincide, which confirms the validity of the effective medium approach for guided waves. It is however of interest for future work to test the validity of our result for any ka value (recall indeed that we assumed $a/H \ll 1$ but not $ka \ll 1$ *a priori*).

V. CONCLUSIONS

We studied the propagation of acoustic waves in a waveguide containing inclusions of any shape and presenting contrasts in wavespeed and in density with respect to the host medium. An iterative modal approach is developed. This allows us to get a numerical scheme (NBC), easy to implement due to implying one-dimensional quantities (the modal components of the two-dimensional field). By comparison with numerical experiments (performed using a finite element method on MELINA code), the method based on the Born approximations is shown to be accurate, even for scattered fields whose amplitudes are of the same order of magnitude as that of the incident wave. This scattered amplitude (ϵ_s) is the relevant parameter for the accuracy of the method, typically accurate in $O(\epsilon_s^2)$ in the first iteration. Until values of ϵ_s close to unity, iterating the NBC produces a convergence of the solution. The ϵ_s-value results from the combined effects of the inclusion size and of the contrasts in density and in wavespeed. This means that no individual limitations applies: Namely, a large inclusion with weak contrasts can produce a small ϵ_s-value. Note also that ϵ_s can be evaluated, in practice, by considering the scattering strength of the same inclusion, or set of inclusions, in free space (this latter quantity is, in general, easier to obtain).

For inclusion sizes R, small compared to the waveguide height H, analytical expressions of the transmission and reflection coefficients are given. Because the restriction concerns the R/H-value only, our predictions hold for any kR-value, which is of particular interest to explore the high frequency regime. This is encapsulated in a factor $\mathcal{S}(kR)$,

that accounts for the shape of the inclusion and for the frequency regime [with $\mathcal{S}(kR) \to 1$ for $kR \to 0$]. Comparison with numerical experiments shows that the results is accurate typically in $O(\epsilon_s^2)O((R/H)^2)$.

The scattering properties of periodically and randomly distributed inclusions have been considered in more detail. The main conclusions are the following. Our approach, being perturbative, is unable to account for resonance effects. This appears in the divergence of p_B near the cutoff frequencies, or equivalently for periodic case in the Wood's anomalies. When compared to other perturbative approaches valid in the low frequency regime, our analytical predictions are less accurate at low frequencies, although iterating the Born approximation in that case causes the solution to converge to the correct solution. In addition, the main advantage of our approach is the validity of our predictions in the high frequency regime.

Future works concern the case of randomly distributed inclusions. By comparing with numerical experiments, it will be possible to explore the bounds of validity of our prediction beyond the low frequency regime. Extension to elasticity is possible, by considering modal expansion on the Lamb modes.

ACKNOWLEDGMENT

This work is supported by the international ANR project Procomedia.

APPENDIX: NUMERICAL IMPLEMENTATION OF THE SUCCESSIVE NBC

$p_{NBC}(x, y)$ is calculated in the successive NBC using the N_{it}-th iteration in Eq. (11) then

$$p_{NBC}(x,y) = \sum_{n-0}^{N_{mod}} p_n^{N_{it}}(x)\psi_n(y), \tag{A1}$$

which depends on (N_{it}, N_{mod}) and is expected to converge when increasing both parameters. The numerical procedure to derive $p_n^{N_{it}}(x)$ is straightforward. We define $A_1 \equiv (\rho/\tilde{\rho} - 1)/H$ and $A_2 \equiv k^2\left(B/\tilde{B} - 1\right)/H$ for simplicity. Initialization is given with $p_n^{(1)}(x_i) = e^{ik_N x_i}\delta_{nN}$ and $p_n^{(1)\prime}(x_i) = ik_N e^{ik_N x_i}\delta_{nN}$. Then, with

$$\begin{aligned} N_1^{(1)}(j,n) &\equiv \sum_m A_1 C_{nm}(x_j) p_m^{(1)\prime}(x_j), \\ N_2^{(1)}(j,n) &\equiv \sum_m \left[A_1 D_{nm}(x_j) - A_2 C_{nm}(x_j)\right] p_m^{(1)}(x_j) \end{aligned} \tag{A2}$$

and a parametrization of the inclusion located between x_1 and x_2, $x_i = x_1 + i\,\Delta x$ with $i = 0,...,N_x$ and $\Delta x = (x_2 - x_1)/N_x$,

$$\begin{aligned} p_n^{(2)}(x_i) &= e^{ik_N x i}\delta_{nN} + \Delta x \sum_j \left[-g_n'(x_i - x_j)N_1^{(1)}(j,n)\right. \\ &\quad \left. + g_n(x_i - x_j)N_2^{(1)}(j,n)\right], \\ p_n^{(2)'}(x_i) &= ik_N e^{ik_N x i}\delta_{nN} - N_1^{(1)}(i,n) \\ &\quad + \Delta x \sum_j \left[k_n^2 g_n(x_i - x_j)N_1^{(1)}(j,n)\right. \\ &\quad \left. + g_n'(x_i - x_j)N_2^{(1)}(j,n)\right]. \end{aligned} \tag{A3}$$

Iteration is done using $p_n^{(1)}(x_i) = p_n^{(2)}(x_i)$ and $p_n^{(1)\prime}(x_i) = p_n^{(2)\prime}(x_i)$. The final x-mesh $X_i = iL/N_x$, $i = 0, \ldots, N_x$ is used after $p_n^{N_{it}-1}(x_j)$ has been calculated

$$\begin{aligned} p_n^{(N_{it})}(X_i) &= e^{ik_N x_i}\delta_{nN} \\ &\quad + \Delta x \sum_j \left[-g_n'(X_i - x_j)N_1^{(N_{it}-1)}(j,n)\right. \\ &\quad \left. + g_n(X_i - x_j)N_2^{(N_{it}-1)}(j,n)\right]. \end{aligned} \tag{A4}$$

[1] N. K. Uzunoglu, "Scattering from inhomogeneities inside a fiber waveguide," J. Opt. Soc. Am. **71**, 259–273 (1981).
[2] I. D. Chremmos and N. K. Uzunoglu, "Analysis of scattering by a linear chain of spherical inclusions in an optical fiber," J. Opt. Soc. Am. **23**, 3054–3062 (2006).
[3] Z. L. Wang and W. G. Lin, "Raman or fluorescent scattering by active molecules or ions embedded in a single mode optical fiber," Appl. Opt. **32**, 6645–6649 (1993).
[4] D. K. Dacol and D. G. Roy, "Wave scattering in waveguides," J. Math. Phys. **44**, 2133–2148 (2003).
[5] A. Thode and K. Kim, "Multiple-order derivatives of a waveguide acoustic field with respect to sound speed, density, and frequency," J. Acoust. Soc. Am. **116**, 3370–3383 (2004).
[6] L. Bourgeois and E. Luneville, "The linear sampling method in a waveguide: A modal formulation," Inverse Probl. **24**, 015018 (2008).
[7] P. Cristini and A. Wirgin, "Identification of the size, proportions and location of a soft body of revolution in a shallow water waveguide," Inverse Probl. **16**, 1727 (2000).
[8] F. D. Philippe, C. Prada, J. de Rosny, D. Clorennec, J.-G. Minonzio, and M. Fink, "Characterization of an elastic target in a shallow water waveguide by decomposition of the time-reversal operator," J. Acoust. Soc. Am. **124**, 779–787 (2008).
[9] I. Lucifredi and H. Schmidt, "Subcritical scattering from buried elastic shells," J. Acoust. Soc. Am. **120**, 3566–3583 (2006).
[10] V. Baronian, A. S. Bonnet-Ben Dhia, and E. Luneville, "Transparent boundary conditions for the harmonic diffraction problem in an elastic waveguide," J. Comp. Appl. Math. **234**, 1945–1952 (2010).
[11] A. S. Bonnet-Bendhia and F. Starling, "Guided waves by electromagnetic gratings and non-uniqueness examples for the diffraction problem," Math. Methods Appl. Sci. **17**, 305–338 (1994).
[12] C. M. Linton, "Schlomilch series that arise in diffraction theory and their efficient computation," J. Phys. A **39**, 3325–3339 (2006).
[13] A. Barnett and L. Greengard, "A new integral representation for quasi-periodic scattering problems in two dimensions," BIT Numer. Math. **51**, 67–90 (2011).
[14] J. D. Joannopoulos, S. G. Johnson, J. N. Winn, and R. D. Meade, *Photonic Crystals. Molding the Flow of Light*, 2nd ed. (Princeton University Press, Princeton, NJ, 2008).
[15] Y. Pennec, B. Djafari Rouhani, H. Larabi, A. Akjouj, J. N. Gillet, J. O. Vasseur, and G. Thabet, "Phonon transport and waveguiding in a phononic crystal made up of cylindrical dots on a thin homogeneous plate," Phys. Rev. B **80**, 144302 (2009).
[16] M. Oudich, M. B. Assouar, and Z. Hou, "Propagation of acoustic waves and waveguiding in a two-dimensional locally resonant phononic crystal plate," Appl. Phys. Lett. **97**, 193503 (2010).
[17] Y. Pennec, J. O. Vasseur, B. Djafari-Rouhani, L. Dobrzynski, and P. A. Deymier, "Two-dimensional phononic crystals: Examples and applications," Surf. Sci. Rep. **65**, 229–291 (2010).
[18] T. G. Mast, A. I. Nachman, and R. C. Waag, "Focusing and imaging using eigenfunctions of the scattering operator," J. Acoust. Soc. Am. **102**, 715–725 (1997).
[19] S. Dediu and J. R. McLaughlin, "Recovering inhomogeneities in a waveguide using eigen-system decomposition," Inverse Probl. **22**, 1227–1246 (2006).
[20] R. P. Gilbert, M. Werby, and Y. Z. Xu, "Determination of a buried object in a two-layered shallow ocean," J. Comp. Acoust. **9**, 1025–1037 (2001).
[21] R. P. Gilbert and Y. Z. Xu, "Acoustic imaging in a shallow ocean with a thin ice cap," Inverse Probl. **16**, 1799–1811 (2000).
[22] W. Kohn, "On the convergence of Born expansions," Rev. Mod. Phys. **26**, 292–310 (1954).
[23] D. N. Ghosh Roy and G. J. Orris, "A Born scatterer in an acoustical waveguide," J. Acoust. Soc. Am. **114**, 626–630 (2003).

[24]D. N. Ghosh Roy, G. J. Orris, and L. S. Couchman, "Born series in obstacle scattering," Appl. Math. Lett. **16**, 205–210 (2003).
[25]S. K. Sharma and R. K. Saha, "On the validity of some new acoustic scattering approximations," Waves Random Complex Media **14**, 525–537 (2004).
[26]H. R. Gordon, "Rayleigh-Gans scattering approximation: Surprisingly useful for understanding backscattering from disk-like particles," Opt. Exp. **15**, 5572–5588 (2007).
[27]I. R. Capoglu, J. D. Rogers, A. Taflove, and V. Backman, "Accuracy of the Born approximation in calculating the scattering coefficient of biological continuous random media," Opt. Lett. **34**, 2679–2681 (2009).
[28]J. Li, X. Wang, and T. Wang, "On the validity of Born approximation," Progr. Electromagn. Res. **107**, 219–237 (2010).
[29]I. Manning, "Error and convergence bounds for the Born expansion," Phys. Rev. **139**, 495–500 (1965).
[30]C. J. Joachain and C. Quigg, "Multiple scattering expansions," Rev. Mod. Phys. **46**, 279–324 (1974).
[31]P. M. A. Sloot and C. G. Fidgor, "Elastic light scattering from nucleated blood cells," Appl. Opt. **25**, 3559–3565 (1986).
[32]A. Aubry and A. Derode, "Multiple scattering of ultrasound in weakly inhomogeneous media: Application to human soft tissues," J. Acoust. Soc. Am. **129**, 225–233 (2011).
[33]For more information on MELINA, see http://homepage.mac.com/danielmartin/melina/ (Last viewed 08/24/11).
[34]R. Porter and D. V. Evans, "Rayleigh-Bloch surface waves along periodic gratings and their connection with trapped modes in waveguides," J. Fluid Mech. **386**, 233–258 (1999).
[35]R. W. Wood, "On a remarkable case of uneven distribution of light in a diffraction grating spectrum," Philos. Mag. **4**, 396–402 (1902).
[36]Lord Rayleigh, "On the dynamical theory of the grating," Proc. R. Soc. London, Ser. A **79**(532), 399–416 (1907).
[37]C. M. Linton and I. Thompson, "Resonant effects in scattering by periodic arrays," Wave Motion **44**, 165–175 (2007).
[38]V. Twersky, "On the scattering of waves by an infinite grating," IEEE Trans. Antennas Propag. **4**, 330–345 (1956).
[39]V. Twersky, "On scattering of waves by the infinite grating of circular cylinders," IEEE Trans. Antennas Propag. **10**, 737–765 (1962).
[40]J. W. Miles, "On Rayleigh scattering by a grating," Wave Motion **4**, 285–292 (1982).
[41]E. Luneville and J.-F. Mercier, "Finite element simulations of multiple scattering in acoustic waveguides," Waves Random Complex Media **20**, 615–633 (2010).
[42]A. Maurel, J.-F. Mercier, and F. Lund, "Elastic wave propagation through a random array of dislocations," Phys. Rev. B **70**, 024303 (2004).
[43]A. Maurel, V. Pagneux, F. Barra, and F. Lund, "Wave propagation through a random array of pinned dislocations: Velocity change and attenuation in a generalized Granato and Lucke theory," Phys. Rev. B **72**, 174111 (2005).
[44]M. Chekroun, L. Le Marrec, B. Lombard, O. Abraham, and J. Piraux, "Comparisons between multiple scattering methods and time-domain numerical simulations for elastic waves," J. Acoust. Soc. Am. **123**, 3845 (2008).
[45]P.-Y. Le Bas, F. Luppé, and J.-M. Conoir, "Reflection and transmission by randomly spaced elastic cylinders in a fluid slab-like region," J. Acoust. Soc. Am. **117**, 1088–1097 (2005).
[46]P. A. Martin, "Multiple scattering by random configurations of circular cylinders: Reflection, transmission, and effective interface conditions," J. Acoust. Soc. Am. **129**, 1685–1695 (2011).
[47]P. A. Martin and A. Maurel, "Multiple scattering by random configurations of circular cylinders: Weak scattering without closure assumptions," Wave Motion **45**, 865–880 (2008).